Chiral porphyrazine near-IR optical imaging agent exhibiting preferential tumor accumulation

Evan R. Trivedi[a], Allison S. Harney[a,b], Mary B. Olive[c], Izabela Podgorski[c], Kamiar Moin[c], Bonnie F. Sloane[c], Anthony G.M. Barrett[d], Thomas J. Meade[a,b], and Brian M. Hoffman[a,1]

[a]Departments of Chemistry and Biochemistry, Molecular Biology, and Cell Biology, Northwestern University, Evanston, IL, 60208; [b]Departments of Neurobiology, Physiology, and Radiology, Northwestern University, Evanston, IL, 60208; [c]Department of Pharmacology and Karmanos Cancer Institute, Wayne State University School of Medicine, Detroit, MI, 48201; and [d]Department of Chemistry, Imperial College of Science, Technology and Medicine, South Kensington, London SW7 2AZ, United Kingdom

Contributed by Brian M. Hoffman, Northwestern University, Evanston, IL, November 9, 2009 (sent for review October 7, 2009)

A chiral porphyrazine (pz), H_2[pz(*trans*-A_2B_2)] (247), has been prepared that exhibits preferential in vivo accumulation in the cells of tumors. Pz 247 exhibits near-infrared (NIR) emission with $\lambda > 700$ nm in the required wavelength range for maximum tissue penetration. When MDA-MB-231 breast tumor cells are treated with 247, the agent shows strong intracellular fluorescence with an emission maximum, 704 nm, which indicates that it localizes within a hydrophobic microenvironment. Pz 247 is shown to associate with the lipophilic core of LDL and undergo cellular entry primarily through receptor-mediated endocytosis accumulating in lysosomes. Preliminary in vivo studies show that 247 exhibits preferential accumulation and retention in the cells of MDA-MB-231 tumors subcutaneously implanted in mice, thereby enabling NIR optical imaging with excellent contrast between tumor and surrounding tissue. The intensity of fluorescence from 247 within the tumor increases over time up to 48 h after injection presumably due to the sequestration of circulating 247/LDL complex by the tumor tissue. As the need for cholesterol, and thus LDL, is elevated in highly proliferative tumor cells over nontumorigenic cells, 247 has potential application for all such tumors.

low-density lipoprotein | molecular imaging | near-IR fluorescence | porphyrinoid | tumor imaging

Survival rates of breast cancer patients might be dramatically improved if we could detect tumors in their early stages (1, 2). The primary technique for early screening for breast cancer, x-ray mammography, is effective, but is susceptible to false positives that require additional, often invasive testing, whereas the exposure to ionizing radiation inherent to x-ray procedures limits the frequency of screening for high-risk patients.

Fluorescence imaging with near-infrared (NIR) contrast agents is an emerging, highly sensitive method for tumor detection (3, 4) that takes advantage of the relative transparency of mammalian tissue to NIR light (approximately 700–900 nm) (5). Used in conjunction with a contrast agent that absorbs and emits in the NIR and accumulates in tumor tissue, this could well provide an ideal, noninvasive detection method for superficial tumors or even those that can be accessed by endoscopy.

Porphyrins, phthalocyanines, and related tetrapyrroles have attracted considerable attention as optical imaging agents as well as photosensitizers for photodynamic therapy (PDT) (6, 7). Porphyrazines (pzs) are a relatively unstudied class of macrocycles that combine some of the features of porphyrins and phthalocyanines (Chart 1), while exhibiting distinctive physical and chemical properties of their own (8). A particular virtue of the pzs is the ease with which one can functionalize the pyrrole carbons of the macrocylic core with heteroatoms. Heteroatom-functionalized pzs have intense NIR absorption/emission (8) and recently have been considered as optical contrast agents for tumor detection and as a platform for cancer treatment using PDT (9, 10). These pzs are synthetically flexible (8), making it possible to independently fine tune their NIR optical characteristics and amphiphilicity, a characteristic shown to dictate tumor retention of porphyrinoids (11, 12).

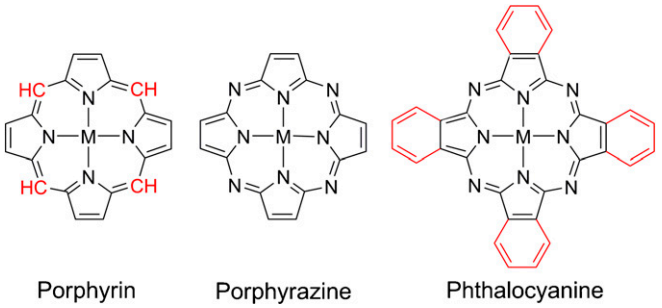

Chart 1.

Herein we report the synthesis and biological properties of the chiral Pz 247 (Fig. 1*A*). We find that 247 is taken up by cells into lysosomes through LDL receptor-mediated endocytosis and that this leads to preferential accumulation in tumor cells in vivo, thereby enabling NIR optical imaging with excellent contrast between tumor and surrounding tissue.

Results

Pz 247 (Fig. 1*A*) , with four homochiral centers attached through oxygen atoms at the periphery of the macrocycle core, was prepared and characterized as described in *Materials and Methods*.

Electronic Absorption and Emission of 247. The optical properties of 247 are similar to those of analogous heteroatom-functionalized pzs, the H_2[pz(*trans*-$\mathbf{A_2B_2}$)] pzs, where **A** and **B** represent two types of moieties appended *trans* to each other on the pz periphery (13, 14); for 247, $\mathbf{A} = (2R, 3R)$ 2,3-dimethyl-2,3-dimethoxy-1,4-diox-2-ene; $\mathbf{B} = \alpha, \alpha'$-diisopropoxy benzo (15). Pz 247 exhibits three major optical absorptions, the Soret band (329 nm) and two NIR Q-bands, $Q_x = 702$ and $Q_y = 629$ nm (Fig. 1*B*).

Pzs exhibit dual fluorescence, much like phthalocyanines (16–18). Thus, 247 has intense NIR emission from the first (S_1) excited singlet state (Fig. 1*B*, $\Phi_f = 0.090$, and Table S1) that can be excited with light of any wavelength throughout its absorption spectrum. With excitation at Q_x or Q_y, 247 presents a favorable combination of NIR absorption and emission characteristics for maximum tissue penetration and optimal in vivo optical imaging. In addition, 247 has intense blue emission from the second (S_2)

Author contributions: E.R.T., A.S.H., K.M., B.F.S., A.G.M.B., T.J.M., and B.M.H. designed research; E.R.T., A.S.H., M.B.O., and I.P. performed research; and E.R.T., A.S.H, T.J.M., and B.M.H. wrote the paper.

The authors declare no conflict of interest.

[1]To whom correspondence should be addressed. E-mail: bmh@northwestern.edu.

This article contains supporting information online at www.pnas.org/cgi/content/full/0912811107/DCSupplemental.

www.pnas.org/cgi/doi/10.1073/pnas.0912811107

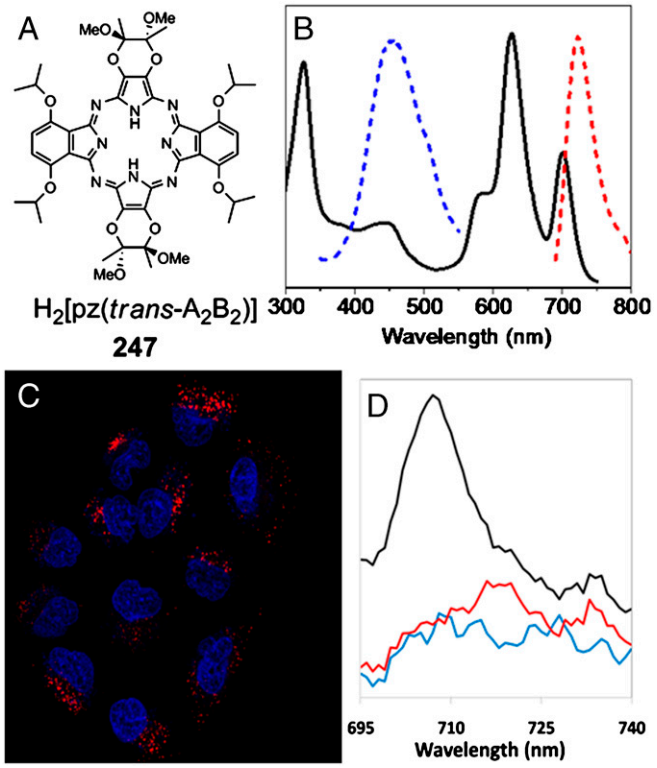

Fig. 1. Absorption and emission of 247. (*A*) Chemical structure of H_2[pz(*trans*-A_2B_2)], 247. (*B*) Absorption spectrum of 247 (black) in CH_2Cl_2 with S_2 (blue) and S_1 (red) emission spectra normalized to fit the scale. (*C*) Intracellular S_1 emission of 247 in A549 lung carcinoma cells imaged by confocal microscopy. Cells in serum-containing medium were treated with 25 μM 247 (red) for 18 h and stained for nuclei (DAPI, blue). Contrast has been slightly adjusted to improve the visualization of the differently stained structures. (*D*) Emission spectra from MDA-MB-231 cells incubated with 247 (black), control MDA-MB-231 cells (blue), and 247 in serum-containing medium (no cells) (red).

excited singlet state ($\lambda_{em} = 462$ nm) (Fig. 1*B*), which provides a convenient means of in vitro monitoring.

The blue S_2 fluorescence of 247 in solution is essentially invariant to solvent polarity, but the NIR fluorescence seen in a nonpolar environment red shifts and becomes quenched as the polarity increases (Table S1) (19, 20). Thus, 247 is a "sensitive fluorophore" (21) whose NIR emission color and intensity provides insight into its microenvironment within a biological system. In addition, when 247 resides in an environment where the Stokes shift relative to Q_x is small, making it difficult to discriminate between S_1 emission and scattered light from Q_x excitation, it can be excited with comparable efficiency in the Q_y band. This introduces a large effective Stokes shift, facilitating precise fluorescence imaging, and we employ this strategy here.

In Vitro Uptake of 247 by Tumor Cells. To test for uptake of 247 by tumor cells, five breast, one lung, and one cervical cancer cell line were incubated with 247, washed, and imaged by confocal microscopy. As illustrated for A549 lung carcinoma cells in Fig. 1*C* and for the others in Fig. S1, all treated cells display intracellular 247 NIR fluorescence with a punctuate subcellular distribution that is absent in untreated cells. Confocal images taken at 0.42 μm increments through a MDA-MB-231 breast tumor cell show that the pz is internalized by the cells and not simply associated with the external cell membrane (Fig. S2). Assays of cellular viability using 3-(4,5-dimethylthiazol-2-yl)-2,5-diphenyl tetrazolium bromide reveal that 247 has no effect on cell growth in the absence of light, but that it exhibits significant phototoxicity as a result of singlet oxygen generation by 247 (22). The emission spectrum of MDA-MB-231 cells treated with 247 has a maximum at 704 nm, the same as for 247 in cyclohexane (Fig. 1*D*), indicating that the incorporated dye is localized in a highly nonpolar subcellular microenvironment.

The punctate staining of 247 was consistent with uptake into a vesicular compartment. To determine the precise location, tumor cells were coincubated with NIR fluorescent 247 and green fluorescent organelle-specific dyes (Fig. S3). The yellow color from colocalized agent and dye when the images are overlaid indicates that the accumulated 247 is present in a subset of lysosomes (Fig. S3*D*), but not in the cytoplasm (Fig. S3*A*), mitochondria (Fig. S3*B*), or endoplasmic reticulum (Fig. S3*C*). Analogous results have been reported for several other porphyrinoid macrocyclic derivatives (23–25).

Mechanism of 247 Accumulation in Tumor Cells. Hydrophobic tetrapyrroles accumulate in cells through a variety of mechanisms, including passive diffusion, entry by flipping through the membrane, and association with serum proteins (11, 26). Serum components, including albumin and LDL, have been shown to act as delivery vehicles for hydrophobic compounds through receptor-dependent and independent endocytosis, both leading to lysosomal accumulation (26–28). To determine whether uptake of 247 is associated with serum components, MDA-MB-231 breast tumor cells were incubated with 247 in complete media (Fig. 2*A*),

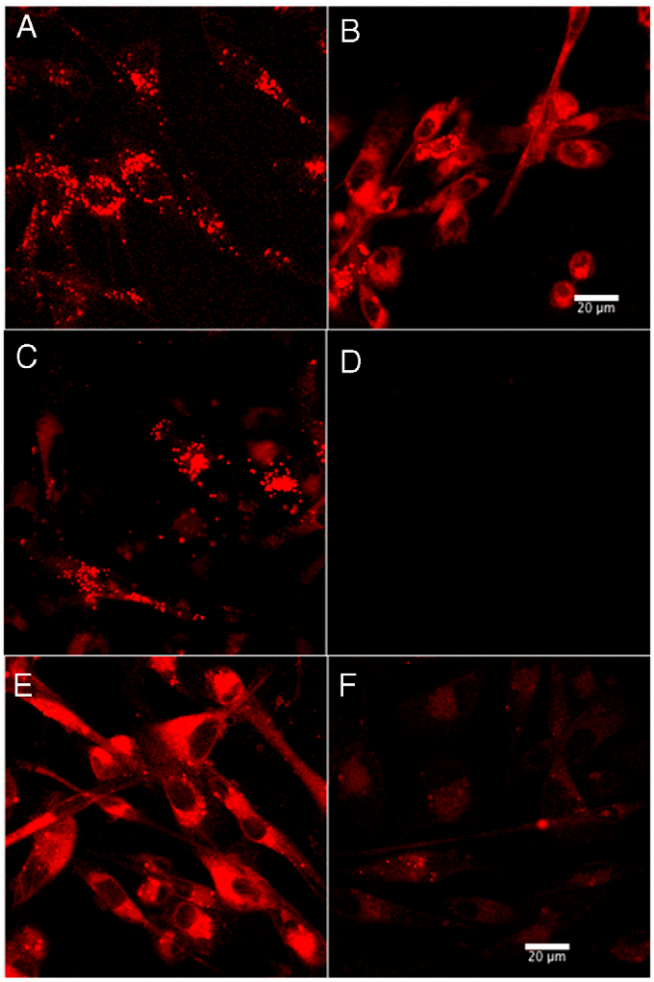

Fig. 2. Serum-dependent vesicular localization of 247. MDA-MB-231 cells incubated with 50 μM 247 for 1 h in the (*A*) presence or (*B*) absence of serum in culture medium. LDL-mediated uptake of 247 in serum-deficient media and inhibition by heparin. MDA-MB-231 cells were incubated with 3 μM 247 in serum-deficient media with (*C*) 100 μg/mL LDL, (*D*) 100 μg/mL LDL and 5 mg/mL heparin, (*E*) 100 μg/mL BSA, and (*F*) 100 μg/mL BSA and 5 mg/mL heparin. (Scale bar, 20 μm.)

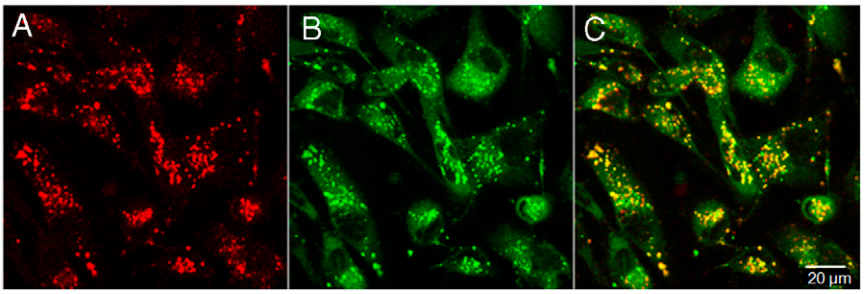

Fig. 3. Colocalization of 247 with LDL. MDA-MB-231 cells incubated with 30 μm 247 and 150 μg/mL LDL-BODIPY for 5 h. (*A*) 247 fluorescence (ex/em: 633 nm/835 ± 135 nm BP). (*B*) BODIPY fluorescence (ex/em: 488 nm/505–530 nm BP). (*C*) Overlaid image of 247 and BODIPY. (Scale bar, 20 μm.)

serum-deficient media in the absence (Fig. 2*B*) or presence of either 100 μg/mL of LDL (Fig. 2*C*) or BSA (Fig. 2*E*). Only when LDL is present did punctate staining occur; otherwise diffuse staining was observed.

To test the possible role of low-density lipoprotein receptor (LDL-R) in cellular uptake of 247, experiments were performed in the presence of heparin, which inhibits LDL binding to LDL-R and also displaces extracellularly bound LDL (29–31). Addition of 25 mg/mL heparin to complete media eliminates the lysosomal localization of 247 (Fig. S4*B*), whereas addition of 5 mg/mL heparin to serum-free media containing 100 μg LDL completely blocks uptake (Fig. 2*D*). This effect of heparin on the staining pattern also was observed with MCF7 and Hs578t breast tumor cells (Fig. S5). These effects are consistent with 247 being taken up through endocytosis mediated by LDL-R. In contrast, the diffuse staining pattern seen with BSA (Fig. 2*E*) was not influenced by the addition of heparin (Fig. 2*F*). It is likely that the diffuse staining seen when LDL is absent reflects the existence of additional passive mechanisms for 247 uptake.

When confocal images from MDA-MB-231 cells coincubated with 247 and human LDL conjugated with a green fluorescent dye [LDL-boron-dipyrromethene (LDL-BODIPY)] are overlaid, the resulting yellow color demonstrates colocalization within the cells (Fig. 3). The spectroscopic evidence (Fig. 1*D*) that 247 localizes in a nonpolar environment within the cell further suggests that 247 associates with the hydrophobic core of LDL. This is confirmed by preliminary FRET measurements, which show that the LDL-BODIPY fluorescence is quenched with an efficiency of approximately 90% by incorporation of 247 into LDL-BODIPY (Fig. S6).

In Vivo Accumulation of 247 in Tumors. To test for preferential in vivo accumulation of 247 in tumors, MDA-MB-231 breast carcinoma cells stably expressing red fluorescent protein (RFP) were implanted subcutaneously in female SCID mice, and the mice were injected with 200 nmol 247 by tail vein. As shown in Fig. 4*A*, RFP fluorescence was imaged 24 h after injection [580–620 nm band pass (BP) filter], RFP-expressing tumors were seen in each flank of the mouse. In the corresponding image, using an NIR filter set for the detection of S_1 emission from 247 (680–720 nm BP), the tumor is clearly visible above a negligible background in the surrounding tissue (Fig. 4*B*). The overlay of the two images (Fig. 4*C*) demonstrates that 247 localizes in the tumors.*

Histological confocal fluorescence images of excised tumors revealed intracellular fluorescence from RFP (Fig. 4*D*) and from 247 (Fig. 4*E*); the orange in the image overlay (Fig. 4*F*) confirms that the 247 colocalizes with RFP. This indicates that 247 accumulates within the tumor cells in vivo and not in the invading immune cells.

Five hours after the administration of 247, the signal from the tumors was barely detectable above background (Fig. 5*A*), but after 24 h the tumor signal was much brighter (Fig. 5*B*), and the brightness of the tumors relative to background continued to increase up to 48 h after injection (Fig. 5*D*). Such behavior is to be expected if 247 circulates at low concentration and in a state with low fluorescence yield (Table S1), is progressively taken up by tumors as the LDL complex, and accumulates in a tumor-cell environment where the fluorescence yield is high.

After 48 h, there was a visible signal from the tail near the site of injection, presumably due to the excessive amount of collagen and cartilage in the tail resulting in nonspecific binding of the dye. To further examine dye distribution, treated mice were killed and their internal organs excised and imaged 72 h after injection (Fig. 5*E*). These images demonstrated that 247 had extensively accumulated in the tumor tissue, but was essentially absent from the kidneys, spleen, heart, and muscle tissue. Weak fluorescence was detected in the liver and the lungs. We presume that this slight accumulation was due to the extensive profusion of these organs with blood (a normal occurrence) leading to a slow and transient uptake of 247.

Discussion

The chiral oxygen-functionalized porphyrazine 247 studied here possesses the intense NIR absorption and emission required of an optical contrast agent, and its large effective Stokes shift permits precise imaging of its fluorescence. In vitro experiments show that this agent accumulates in multiple tumor-cell lines, and that the incorporated 247 resides in a hydrophobic intracellular microenvironment. They further show that 247 associates with the lipophilic core of LDLs and undergoes cellular entry primarily by receptor-mediated endocytosis with accumulation in lysosomes.

Preliminary in vivo studies reveal that 247 exhibits preferential accumulation and retention in the tumor cells of MDA-MB-231 human breast tumor xenografts subcutaneously implanted in mice, with strong emission from the tumors, whereas the background signal from other tissue is low. In agreement with the proposed uptake mechanism, the fluorescence intensity at the site of the tumor increased over time as the 247/LDL complex was sequestered in tumor tissue. As the need for LDL-bound cholesterol is elevated in highly proliferative tumor cells over nontumorigenic cells, 247 has a potential application for any highly proliferative tumor (32–35). Alternatively, 247 and other pzs bind to lipid vesicle models (14, 22) that can act as delivery vehicles to tumors (36).

Further optimization of the amphiphilicity, and thus deliverability and uptake of 247 can be achieved by varying the peripheral pz substituents without altering its favorable photophysical properties. Enhanced phototoxicity for PDT applications can be achieved by simply inserting Zn in the pz core, thereby increasing the quantum yield for singlet oxygen formation (37). The favorable NIR optical properties, biocompatibility, in vivo tumor accumulation, and retention of 247 demonstrate that it provides an attractive platform for the development of optical contrast and

*The slight lack of complete colocalization is likely due in part to a difference in the physics of light propagation at the two wavelengths through tissue and fur, and in part to presence of 247 both in the tumor itself and in adjacent areas; the RFP, on the other hand, is expressed in and confined to the tumor cells.

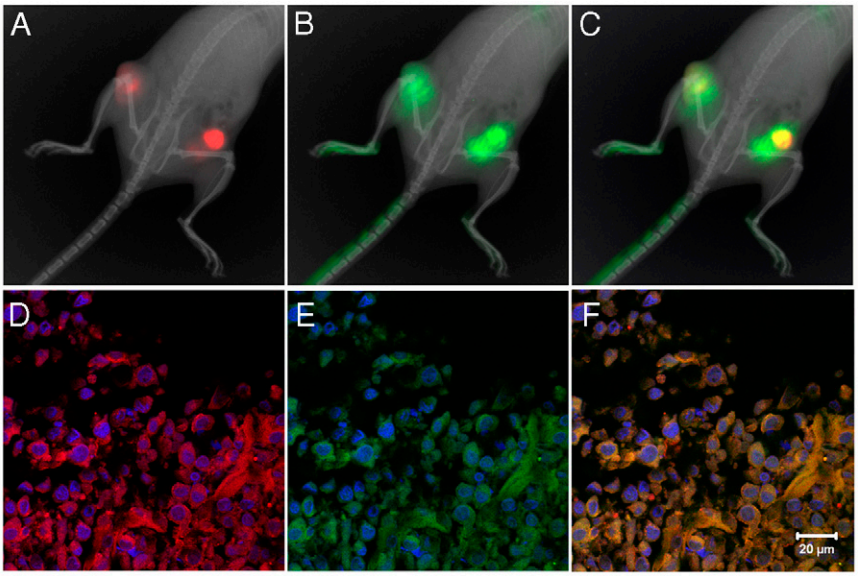

Fig. 4. Porphyrazine 247 accumulated in tumors in vivo. Mice bearing MDA-231 human breast xenograft tumors expressing RFP were administered 200 nmol of 247 by tail-vein i.v. Twenty four hours after injection, live animals were imaged for (*A*) RFP and (*B*) 247. (*C*) Overlay of (*A*) and (*B*). X-ray images were obtained for anatomical coregistration (*A–C*). Confocal microscopy of histological sections of tumors; (*D*) RFP image, (*E*) 247 image, and (*F*) overlay of (*D*) and (*E*). Nuclei were stained with DAPI (blue). (Scale bar, 20 μm.)

even therapeutic agents based on the chemically and photophysically flexible pz system.

Materials and Methods

Porphyrazine Synthesis. Porphyrazine $H_2[pz(trans\text{-}A_2B_2)]$ 247 was prepared (Scheme 1) by cocyclization of (5R, 6R)2,3-dicyano-5,6-dimethoxy-5,6-dimethyl-1,4-diox-2-ene (1) (38) and 4,7-bis(isopropyloxy)-1, 3-diiminoisoindoline (2) (39, 40), with subsequent purification by silica-gel column chromatography, following a modification of a literature procedure (22) (*SI Materials and Methods*).

$H_2[pz(trans\text{-}A_2B_2)]$, 247 (17 mg, 8% yield). TLC (CH_2Cl_2 : EtOAc, 9 : 1 vol/vol): $R_f = 0.63$; UV-visible (CH_2Cl_2) λ_{max} (log ϵ) 329 (4.33), 442 (3.78), 629 (4.40), 702 (4.12) nm; ^{1}H NMR (500 MHz, $CDCl_3$) δ 7.54 (*s*, 4H), 5.61 (*m*, $J = 5.9$ Hz, 4H), 3.58 (*s*, 12H), 2.11 (*s*, 12H), 1.93 (*d*, $J = 5.9$ Hz, 12H), 1.84 (*d*, $J = 5.9$ Hz, 12H); ^{13}C NMR (125 MHz, $CDCl_3$) δ 157.84, 150.73, 136.60, 134.67, 131.80, 123.87, 102.38, 75.34, 49.99, 23.05, 23.00, 18.06; MALDI-MS (*m/z*) calculated for $C_{48}H_{59}N_8O_{12}[M + H]^+$ 940.0, found 941.0.

Fluorescence Microscopy. In general, cells were plated on glass coverslips and grown to 70% confluence. Porphyrazine 247 was administered from a 5 mM dimethyl sulfoxide (DMSO) stock solution and incubated as described in figure legends and *Results*. After the incubation period, the media was removed and replaced with culture media for the indicated time. For all live-cell imaging experiments, cells were washed twice with 1 × PBS and the slide prepared for imaging using imaging buffer to maintain pH (41). NIR fluorescence of 247 was detected using a 835 ± 135 nm BP filter (excitation, 633 nm). All green fluorescence was detected using a 505–535 nm BP filter (excitation, 488 nm). The details of in vitro confocal imaging experiments are described in *SI Text*.

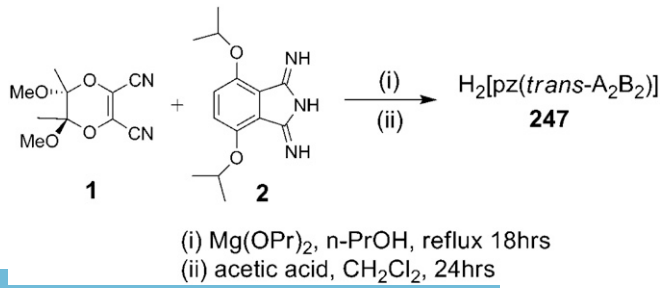

Scheme 1.

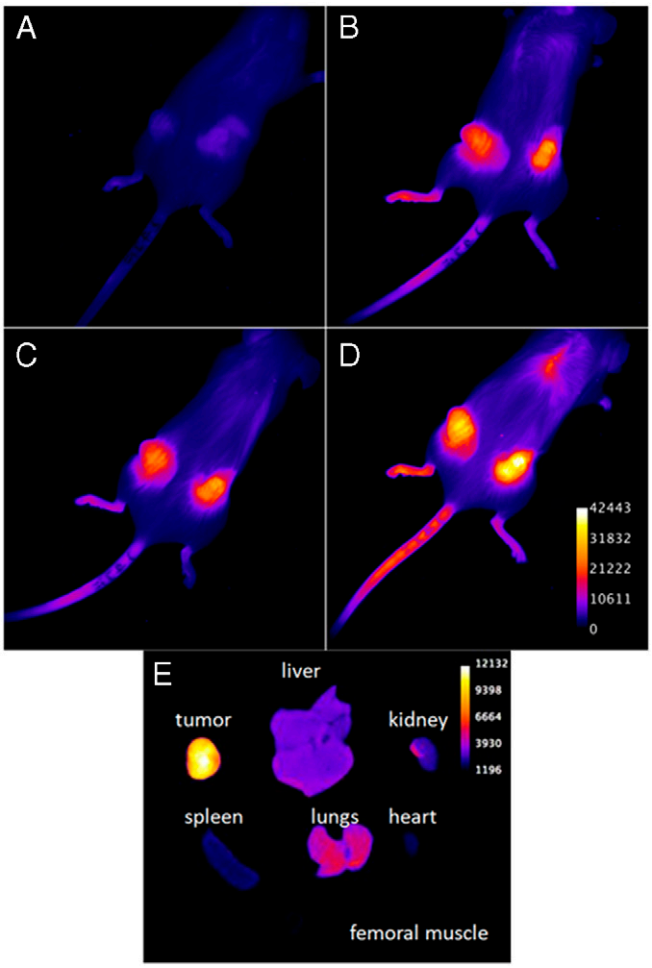

Fig. 5. Accumulation of 247 in tumors over time. Mice bearing MDA-231 human breast xenograft tumors expressing RFP were administered 200 nmol of 247 by tail-vein i.v. Images were acquired (*A*) 5 h, (*B*) 24 h, (*C*) 32 h, and (*D*) 48 h after injection. (*E*) Biodistribution of 247 72 h after injection. From left, (*Top*) tumor, liver, kidney, (*Middle*) spleen, lungs, heart, and (*Bottom*) femoral muscle (no fluorescence).

In Vivo Tumor Imaging. MDA-MB-231 cells (5×10^5) stably expressing RFP were subcutaneously injected into the flanks of 6-week-old female SCID mice ($n = 5$). Tumors were grown for 4 weeks to a size of approximately 1 cm^3. Porphyrazine 247 (200 nmol in 150 μL of distilled H_2O) was administered via tail-vein injection. Solutions for injection were prepared from a 5 mM stock solution of 247 in DMSO. Vehicle control animals were injected with an equivalent amount of DMSO in water. Images were collected after injection at various time intervals as described in figure legends. Each animal was imaged consecutively for pz (625 ± 20 nm excitation, 700 ± 20 nm emission) and RFP (535 ± 20 nm excitation, 600 ± 20 nm emission), as well as an x-ray for anatomical coregistration using a Kodak IS4000MM small animal multimodal imaging system.

ACKNOWLEDGMENTS. This work was supported by the Penny Severns Research Fund (B.M.H.), by the National Science Foundation Nanoscale Science and Engineering Initiative Grant EEC-0647560 (to B.M.H.); the National Institutes of Health (NIH) Grant CA56586 (to B.F.S.); NIH Grant EB005866 (to T.J.M.); NIH Grants P30 CA22453 and P30 ES 06639, and by U54 RR02084330 to B.F.S. and K.M.); and by the Natural Sciences and Engineering Research Council of Canada graduate fellowship (A.S.H.).

1. Alexander FE, et al. (1999) 14 years of follow-up from the Edinbugh randomised trial of breast-cancer screening. *Lancet*, 353(9168):1903–1908.
2. Sant M, et al. (2004) Breast carcinoma survival in Europe and the United States—A population-based study. *Cancer*, 100(4):715–722.
3. Weissleder R (2006) Molecular imaging in cancer. *Science*, 312(5777):1168–1171.
4. Montet X, Ntziachristos V, Grimm J, Weissleder R (2005) Tomographic fluorescence mapping of tumor targets. *Cancer Res*, 65(14):6330–6336.
5. Quaresima V, Matcher SJ, Ferrari M (1998) Identification and quantification of intrinsic optical contrast for near-infrared mammography. *Photochem Photobiol*, 67(1):4–14.
6. Pandey RK, et al. (2006) Nature: A rich source for developing multifunctional agents. Tumor-imaging and photodynamic therapy. *Laser Surg Med*, 38(5):445–467.
7. Ghoroghchian PP, et al. (2005) Near-infrared-emissive polymersomes: Self-assembled soft matter for in vivo optical imaging. *Proc Natl Acad Sci USA*, 102(8):2922–2927.
8. Michel SLJ, Baum S, Barrett AGM, Hoffman BM (2001) Peripherally functionalized porphyrazines: Novel metallomacrocycles with broad, untapped potential. *Prog Inorg Chem*, 50:473–590.
9. Fuchter MJ, Zhong C, Zong H, Hoffman BM, Barrett AGM (2008) Porphyrazines: Designer macrocycles by peripheral substituent change. *Aust J Chem*, 61:235–255.
10. Lee S, et al. (2008) Synthesis and biological analysis of thiotetra (ethylene glycol) monomethyl ether-functionalized porphyrazines: Cellular uptake and toxicity studies. *Metal-Based Drugs*, 2008:391418.
11. Osterloh J, Vicente MGH (2002) Mechanisms of porphyrinoid localization in tumors. *J Porphyr Phthalocya*, 6(5):305–324.
12. Maziere JC, et al. (1990) Cellular uptake and photosensitizing properties of anticancer porphyrins in cell membranes and low and high density lipoproteins. *J Photoch Photobio B*, 6(1-2):61–68.
13. Kobayashi N, Konami H (1996) Molecular orbitals and electronic spectra of phthalocyanine analogues. *Phthalocyanines: Properties and Applications*, , ed Leznoff CC (VCH, New York), Vol 4, pp 343–404.
14. Sholto A, Lee S, Hoffman BM, Barrett AGM, Ehrenberg B (2008) Spectroscopy, binding to liposomes and production of singlet oxygen by porphyrazines with modularly variable water solubility. *Photochem Photobiol*, 84(3):764–773.
15. Michel SLJ, Hoffman BM, Baum SM, Barrett AGM (2001) Peripherally functionalized porphyrazines: Novel metallomacrocycles with broad, untapped potential. *Prog Inorg Chem*, 50:473–590.
16. Kaneko Y, et al. (1997) Violet emission observed from phthalocyanines. *J Photoch Photobio A*, 106(1–3):177–183.
17. Tokumaru K (2001) Photochemical and photophysical behaviour of porphyrins and phthalocyanines irradiated with violet or ultraviolet light. *J Porphyr Phthalocya*, 5(1):77–86.
18. Chahraoui D, Valat P, Kossanyi J (1992) Fluorescence of phthalocyanines—emission from an upper excited-state. *Res Chem Intermediat*, 17(3):219–232.
19. Kawski A (2002) On the estimation of excited-state dipole moments from solvatochromic shifts of absorption and fluorescence spectra. *Z Naturforsch A*, 57a(5):255–262.
20. Mataga N, Kaifu Y, Koizumi M (1956) Solvent effects upon fluorescence spectra and the dipole moments of excited molecules. *B Chem Soc Jpn*, 29:465–470.
21. Slavik J (1982) Anilinonaphthalene sulfonate as a probe of membrane-composition and function. *Biochim Biophys Acta*, 694(1):1–25.
22. Trivedi ER, et al. (2009) Chiral bis-acetal porphyrazines as near-infrared optical agents for detection and treatment of cancer. *Photochem Photobiol* In Press.
23. Zheng X, et al. (2009) Conjugation of 2-(1′-Hexyloxyethyl)-2-devinylpyropheophorbide-a (HPPH) to carbohydrates changes its subcellular distribution and enhances photodynamic activity in vivo. *J Med Chem*, 52:4306–4318.
24. Bonneau S, Morliere P, Brault D (2004) Dynamics of interactions of photosensitizers with lipoproteins and membrane-models: Correlation and cellular incorporation and subcellular distribution. *Biochem Pharmacol*, 68:1443–1452.
25. Woodburn KW (2001) Intracellular localization of the radiation enhancer motexifin gadolinium using interferometric fourier fluorescence microscopy. *J Pharmacol Exp Ther*, 297(3):888–894.
26. Bronshtein I, et al. (2006) In vitro and in vivo photosensitization by protoporphyrins possessing different lipophilicities and vertical localization in the membrane. *Photochem Photobiol*, 82(5):1319–1325.
27. Callahan DE, et al. (1999) Boronated protoporphyrin (BOPP): Localization in lysosomes of the human glioma cell line SF-767 with uptake modulated by lipoprotein levels. *Int J Radiat Oncol Biol Phys*, 45(3):761–771.
28. Bonneau S, Morliere P, Brault D (2004) Dynamics of interactions of photosensitizers with lipoproteins and membrane-models: Correlation with cellular incorporation and subcellular distribution. *Biochem Pharmacol*, 68(7):1443–1452.
29. Goldstein JL, Basu SK, Brunschede GY, Brown MS (1976) Release of low density lipoprotein from its cell surface receptor by sulfated glycosaminoglycans. *Cell*, 7(1):85–95.
30. Krisko A, et al. (2006) The effect of heparin on structural and functional properties of low density lipoproteins. *Biophys Chem*, 119(3):234–239.
31. Brown MS, Goldstein JL (1986) A receptor-mediated pathway for cholesterol homeostasis. *Science*, 232(4746):34–47.
32. Wu SP, et al. (2005) Near-infrared optical imaging of B16 melanoma cells via low-density lipoprotein-mediated uptake and delivery of high emission dipole strength tris[(porphinato)zinc(II)] fluorophores. *Bioconjugate Chem*, 16(3):542–550.
33. Misawa J, et al. (2005) The role of low-density lipoprotein receptors in sensitivity to killing by photofrin-mediated photodynamic therapy in cultured human tumor cell lines. *J Dermatol Sci*, 40(1):59–61.
34. Lo EHK, Ooi VEL, Fung KP (2002) Circumvention of multidrug resistance and reduction of cardiotoxicity of doxorubicin in vivo by coupling it with low density lipoprotein. *Life Sci*, 72(6):677–687.
35. Bonneau S, Vever-Bizet C, Mojzisova H, Brault D (2007) Tetrapyrrole-photosensitizers vectorization and plasma LDL: A physico-chemical approach. *Int J Pharm*, 344(1-2):78–87.
36. Dass CR (2008) Drug delivery in cancer using liposomes. *Drug Delivery Systems*, Methods in Molecular Biology (Humana Press, Clifton, NJ), Vol 437, pp 177–182.
37. Lee S, Stackow R, Foote CS, Barrett AGM, Hoffman BM (2003) Tuning the singlet oxygen quantum yield of near-IR-absorbing porphyrazines. *Photochem Photobiol*, 77(1):18–21.
38. Bellec N, et al. (2000) Porphyrazinediols: Synthesis, characterization, and complexation to group IVB metallocenes. *J Org Chem*, 65(6):1774–1779.
39. Lee S, White AJP, Williams DJ, Barrett AGM, Hoffman BM (2001) Synthesis of near-IR absorbing/emitting porphyrazine derivatives with tunable solubility. *J Org Chem*, 66(2):461–465.
40. Forsyth TP, et al. (1998) A facile and regioselective synthesis of trans-heterofunctionalized porphyrazine derivatives. *J Org Chem*, 63(2):331–336.
41. Brown PS, et al. (2000) Definition of distinct compartments in polarized Madin–Darby canine kidney (MDCK) cells for membrane-volume sorting, polarized sorting and apical recycling. *Traffic*, 1(2):124–140.